ACS Medicinal Chemistry Letters

pubs.acs.org/acsmedchemlett
Letter

Structural and Mechanistic Insights into Atypical Bacterial Topoisomerase Inhibitors

Published as part of ACS Medicinal Chemistry Letters special issue "Structural Biology in Drug Discovery and Development".

Paul D. Toth,[⊥] Steven C. Ratigan,[⊥] Joshua W. Powell, Sydney R. Cassel, Jack C. Yalowich, Craig A. McElroy, Steffen Lindert, Charles E. Bell, and Mark J. Mitton-Fry*

Cite This: ACS Med. Chem. Lett. 2025, 16, 660−667

Read Online

ACCESS | Metrics & More | Article Recommendations | Supporting Information

ABSTRACT: Novel bacterial topoisomerase inhibitors (NBTIs) targeting DNA gyrase and topoisomerase IV constitute a new antibacterial class for deadly pathogens such as MRSA. While most NBTIs induce gyrase-mediated single-strand DNA breaks, a subset of amide NBTIs induces both single-strand and double-strand DNA breaks. Here, we report the X-ray crystal structures of two such amide NBTIs, **148** and **185**, and demonstrate an unusual binding mode characterized by engagement of both GyrA D83 and R122. The synthesis of two isosteric triazole NBTIs is also described, one of which (**342**) affords only single-strand DNA breaks, while the other (**276**) also induces both single- and double-strand DNA breaks. A combination of docking and molecular dynamics simulations is employed to further investigate the potential structural underpinnings of differences in DNA cleavage.

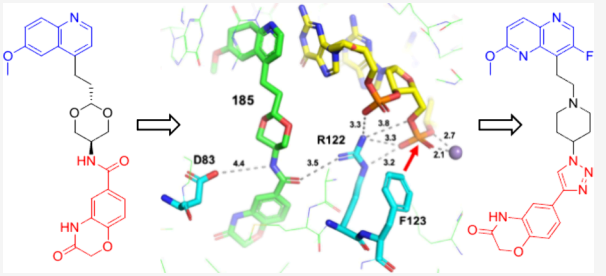

KEYWORDS: *gyrase, amide, triazole, crystallography, molecular dynamics*

Combatting antimicrobial resistance (AMR) and its devastating impact on human health remains a top global priority. Indeed, recent estimates indicate that ∼ 1.3 million individuals die each year as a direct consequence of bacterial AMR.[1] *Staphylococcus aureus*, especially methicillin-resistant strains (MRSA), constitutes the deadliest of the Gram-positive pathogens, and we have a longstanding research program aimed at new therapies for this pathogen.

Our research has focused on Novel Bacterial Topoisomerase Inhibitors (NBTIs),[2,3] small-molecule antibacterial agents targeting the clinically validated enzymes DNA gyrase and topoisomerase IV. These essential enzymes, constituted as A_2B_2 heterotetramers, modulate changes to the topology of bacterial DNA through the intermediacy of transient double-strand breaks to the DNA double helix.[4] In 2010, Bax et al. published the ternary X-ray crystal structure of the NBTI GSK299423, DNA gyrase, and a short segment of double-strand DNA, a true watershed moment for the field.[5] The authors identified a unique ligand binding mode on the 2-fold axis of the GyrA dimer interface. These results immediately rationalized the absence of cross-resistance with existing gyrase inhibitors such as the fluoroquinolones and have stimulated numerous additional structural studies,[6] including with the most clinically advanced NBTI, gepotidacin.[7,8] Other innovative research has elucidated a bifurcated halogen bond employed by some NBTIs,[9,10] further demonstrating the profound impact of structural biology on this emerging class of antibacterials.

The majority of early NBTIs, including GSK299423[5] and gepotidacin,[7] employ a secondary amine (Figure 1A, circled) as a key pharmacophoric element. The basic amine engages an acidic aspartate residue (D83 in *S. aureus* DNA GyrA). The importance of this interaction has been substantiated by several published structures[6] as well as by mutational studies whereby the D83N amino acid substitution commonly drives resistance to NBTIs.[11−14] More recently, several groups have developed nonamine-based NBTIs, most especially amides[15−18] and oxazolidinone-containing compounds.[19−22] Recent crystallographic[20] and computational modeling studies[22] indicated a distinctive binding mode for the oxazolidinones, including interactions with R122 (*S. aureus* numbering), a basic residue directly adjacent to the catalytic tyrosine of DNA gyrase. In contrast, the X-ray crystal structure of one amide-type NBTI revealed a classical interaction with D83.[23] Herein, we report the first ternary X-ray structures of amide

Received: January 31, 2025
Revised: March 19, 2025
Accepted: March 25, 2025
Published: April 1, 2025

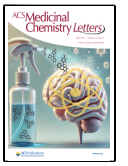

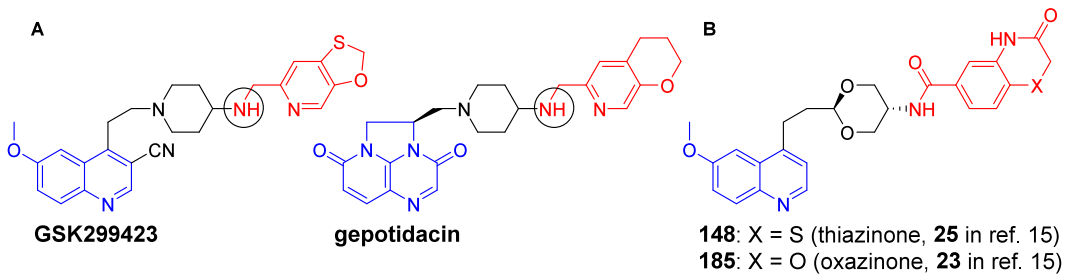

Figure 1. (A) Chemical structures of NBTIs bearing a secondary amine (circled). Blue represents the DNA-binding moiety, black the linker, and red the gyrase-binding moiety. (B) Chemical structures of amide NBTIs with unusual binding mode.

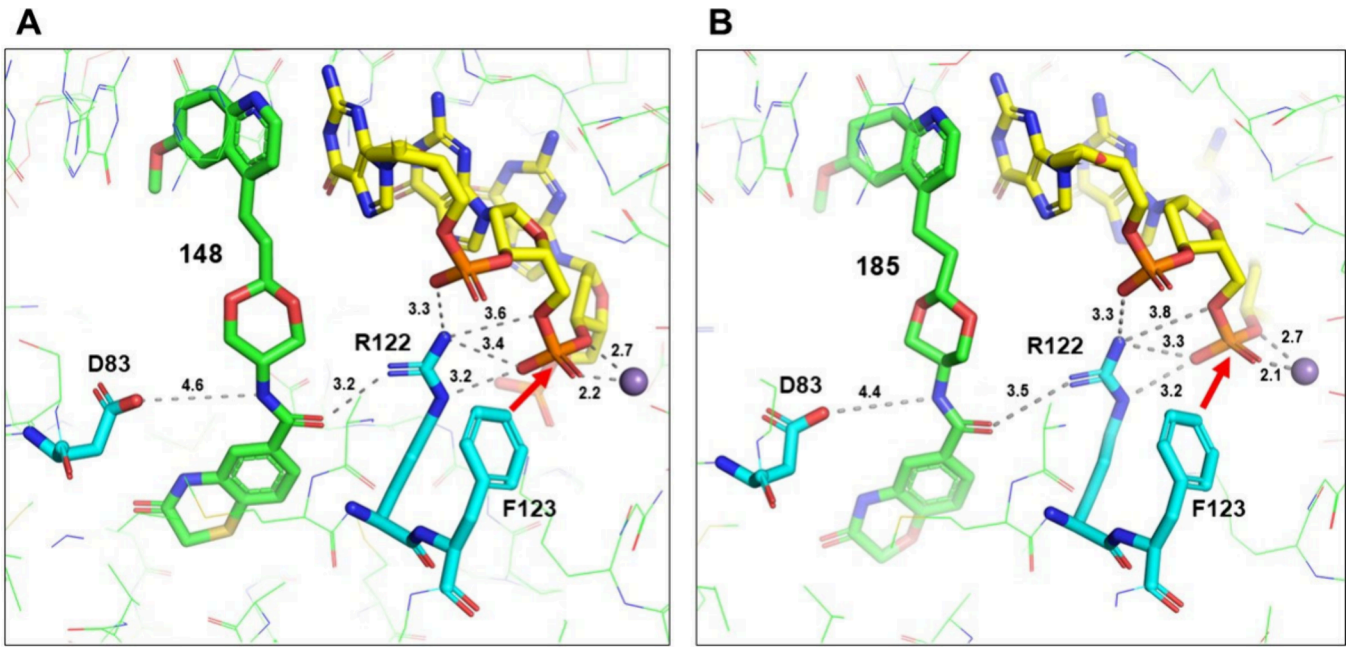

Figure 2. Close-up view of interactions involving compounds **148** (A) and **185** (B). The full structure is shown in thin lines with carbon bonds in green, oxygen in red, nitrogen in blue, and sulfur in yellow. Compounds **148** and **185** are shown in thicker lines. Key gyrase side chains and DNA nucleotides are also shown as thick lines, with carbon bonds in cyan and yellow, respectively. Hydrogen bonds and other electrostatic interactions are shown as dashed lines with distances labeled. Notice that the amide groups of **148** and **185** have their dipole moments interacting favorably in a nearly linear arrangement with D83 on one side and R122 on the other. R122 also forms extensive interactions with the scissile phosphate and the adjacent phosphate in the 3′-direction. The red arrow indicates where the hydroxyl of Y123, if present (but mutated to F), would react with the phosphate that is cleaved.[26] The Mn^{2+} atom is shown as a purple sphere.

NBTIs **148** and **185** (Figure 1B, 2) bound to DNA gyrase and double-stranded DNA with a distinctive binding mode engaging both D83 and R122. These studies spurred the design and synthesis of additional novel chemotypes, including isosteric substitution of the amide moiety by a triazole. Computational docking and molecular dynamics simulations were also employed in an effort to discern a structural rationale for differences in DNA cleavage outcomes.

Inhibition of the hERG cardiac potassium ion channel has presented a significant obstacle to the advancement of the NBTIs.[24] We[15,16] and others[17] have explored replacement of the prototypical secondary amine with a nonbasic amide as one strategy to overcome this liability. Indeed, compounds **148** and **185** (Figure 1B) showed reduced hERG inhibition relative to analogous amine NBTIs.[15] More intriguingly, these two amides and other structurally related analogues led to accumulation of both single- and double-strand DNA breaks in the presence of *S. aureus* gyrase,[15,16] in contrast with the canonical view that NBTIs cause only single-strand breaks.[6] We hypothesized that differential interactions with the enzyme may contribute to this noncanonical NBTI mechanism and thus initiated structural studies.

Crystal structures of **148** and **185** were determined in complex with the *S. aureus* GyrB27−A56(GKdel) Y123F fusion construct[5] with a 20 bp symmetric DNA duplex at resolutions of 1.97 and 2.25 Å, respectively (Figures 2A and 2B). Compounds **148** and **185** differ based on the presence of sulfur or oxygen in the terminal ring of the gyrase-binding moiety (Figure 1B, thiazinone and oxazinone, respectively) and form nearly identical interactions with the gyrase-DNA complex. As expected, both structures contain uncleaved DNA with a single Mn^{2+} ion at the 3′(A) site of each active site.[25,26] The **148** and **185** compounds are each bound along the noncrystallographic 2-fold axis of the gyrase dimer, with the LHS wedging into the central base pairs of the DNA and the RHS binding into the usual hydrophobic pocket formed by the side chains of I70, V71, and M75. Both **148** and **185** are bound as a mixture of two alternative overlapping conformations along the 2-fold axis (Supporting Information Figure S1), as is

https://doi.org/10.1021/acsmedchemlett.5c00060
ACS Med. Chem. Lett. 2025, 16, 660−667

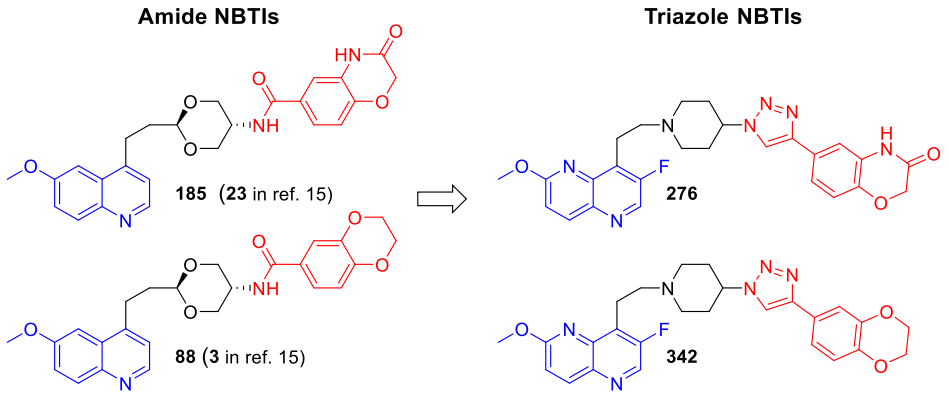

Figure 3. Triazole-containing NBTIs as isosteres of amide-type NBTIs. Notably, **276** and **342** employ a piperidine linker moiety in place of the dioxane linker for ease of synthesis and a fluoronaphthyridine DNA-binding motif in place of a quinoline.

commonly seen for other NBTIs.[6] Only one conformation is shown for the sake of clarity.

As compared to other NBTIs, the linker regions of **148** and **185** are bowed away from the 2-fold axis (Supporting Information Figure S1), which allows them to form additional interactions with the protein. Specifically, the amide groups of **148** and **185** are each bound with their dipole moments nearly colinear with the carboxylate group of D83 on one side (4.4−4.6 Å from the amide nitrogen) and the guanidino group of R122 on the other (3.2−3.5 Å from the amide carbonyl oxygen). The amides are thus positioned to form close to ideally favorable colinear charge-dipole interactions with D83 and R122. The guanidino group of R122 in turn forms a network of H-bonds with the scissile phosphate bound by the Mn^{2+} ion and with the adjacent phosphate in the 3′-direction. In contrast, the dioxane rings of the **148** and **185** linker regions do not form direct interactions with residues of the protein or DNA and are less well-ordered in the structures. The close interactions of the amide groups of **148** and **185** with R122, a key active site residue that contacts the known scissile phosphate to stabilize the excess negative charge of the transition state, suggest a possible mechanism for how **148** and **185** could influence the formation of DNA breaks. Oxazolidinone-type inhibitors have also been shown to engage the R122 residue,[20,22] although published details are lacking as to the stabilization of cleaved DNA by these compounds. Earlier research from Germe et al. demonstrated that an R122A variant of *S. aureus* DNA gyrase is not cleavage-competent.[27]

It is thus tempting to speculate that this unusual binding mode may play a role in the stabilization of double-strand breaks by amides **148** and **185**. However, several additional amide inhibitors afforded only single-strand DNA breaks, including compound **88**[15] (Figure 3). However, our efforts to date have not afforded high-quality crystals with such compounds, leaving open questions about the potential relevance of the interactions with R122. As noted above, the effects of the oxazolidinones[20,22] on DNA cleavage have not been reported. In an effort to bridge this knowledge gap, we undertook additional design and synthesis efforts.

Isosteric substitution is a commonly employed technique in medicinal chemistry, and triazoles constitute an attractive, readily accessible amide bioisostere.[28] Compounds **276** and **342** (Figure 3) were synthesized (Scheme S1, Supporting Information) as isosteric analogues of **185** and **88**, respectively. We hypothesized that the oxazinone-containing **276** would stabilize both DSBs and SSBs in the presence of DNA gyrase, whereas benzodioxane-containing **342** would afford only SSBs based on analogy with the benzodioxane moiety of **88** and its lack of induction of DSBs.[15] DNA cleavage assays were thus conducted using a negatively supercoiled DNA substrate with *S. aureus* DNA gyrase to determine the extent to which SSBs and DSBs were formed.

Incubation of pBR322 DNA with the oxazinone-triazole **276** in the presence of DNA gyrase resulted in a concentration-dependent increase in both SSBs and DSBs (Figure 4), in line

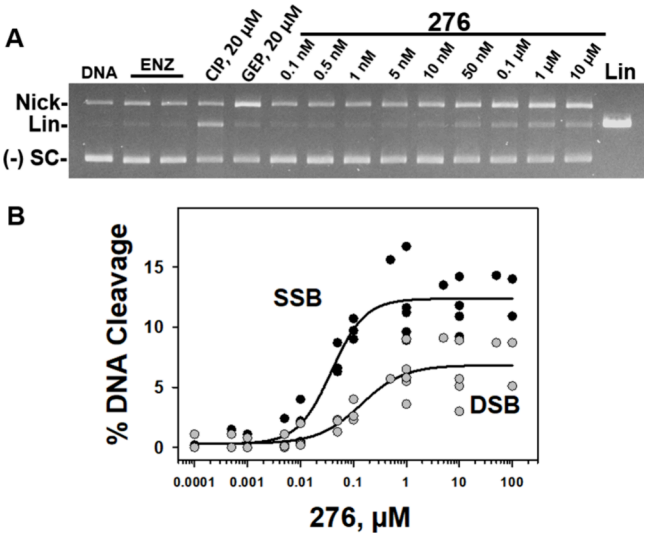

Figure 4. Compound **276** induction of DNA strand breaks in the presence of gyrase. (A) The ethidium-stained gel indicates positions of DNA after incubation with enzyme in the absence or presence of **276** (0.1 nM-10 μM). The various DNA forms are indicated as negatively supercoiled pBR322 DNA substrate ((−)SC), linearized DNA (Lin) representing double-strand breaks, and nicked open-circular DNA (Nick) representing single-strand breaks. Ciprofloxacin and gepotidacin were included as controls at the indicated concentrations. (B) Induction of single strand breaks (SSB) and double-strand breaks (DSB) induced by **276** (0.1 nM-100 μM). Percent DNA cleavage was calculated by assessment of the intensity of DNA bands relative to the intensity of the EcoR1 digested pBR322 band as described in Supporting Information. The percent DNA cleavage in enzyme controls was subtracted to yield the final results. Results shown are derived from 5 separate experiments run on separate days. Regression lines were generated using a 4-logistic curve fit in Sigmaplot 16 (Grafiti LLC, Palo Alto, CA).

https://doi.org/10.1021/acsmedchemlett.5c00060
ACS Med. Chem. Lett. 2025, 16, 660−667

with our hypothesis based on activity of the oxazinone-amide **185**.[15] The maximal percentage of SSBs approached 10−13%, whereas DSBs were somewhat lower (~5−7%). The controls behaved as expected, with ciprofloxacin affording DSBs and gepotidacin yielding SSBs.

The level of SSBs induced by benzodioxane-triazole **342** was similar to that with **276**, but only small quantities of DSBs were formed (Figure 5). These results mirror those seen with

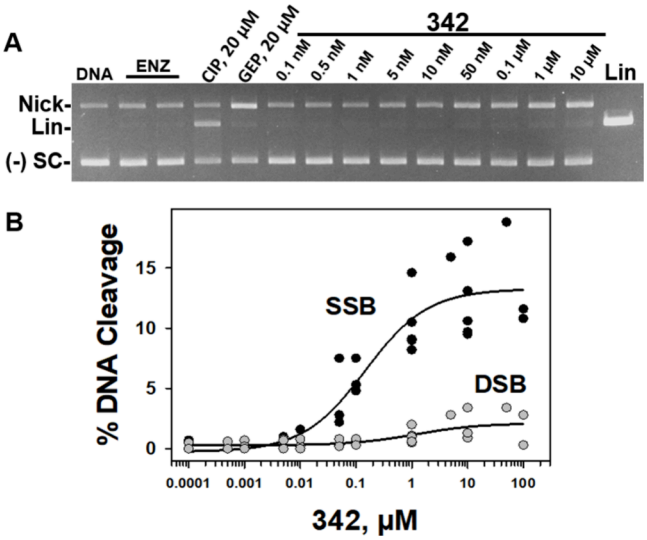

Figure 5. Compound **342** induction of DNA strand breaks in the presence of gyrase. (A) The ethidium-stained gel indicates positions of DNA after incubation with enzyme in the absence or presence of **342** (0.1 nM-10 μM). Ciprofloxacin and gepotidacin were included as controls at the indicated concentrations. (B) Induction of single strand breaks (SSB) and double-strand breaks (DSB) by **342** (0.1 nM-100 μM) was quantified by the same method as that explained in Figure 4. Results shown are derived from 5 separate experiments run on separate days. Regression lines were generated using a 4-logistic curve fit in Sigmaplot 16 (Grafiti LLC, Palo Alto, CA).

amides **185** and **88**,[15] reinforcing the importance of the right-hand side terminal ring. These observations have prompted a more comprehensive program surrounding these triazole NBTIs, the results of which will be reported in due course. We have been unable to obtain high-quality crystals with triazole NBTIs in ternary complexes with DNA gyrase and bacterial DNA.

To facilitate a deeper understanding of the binding modes of nonamine-containing NBTIs, and to attempt to explain the notable differences in DNA cleavage patterns within this subclass of NBTIs, we performed a docking analysis. Using the higher-resolution *S. aureus* DNA gyrase crystal structure resolved with compound **148** as our starting point, we prepared a model system by splitting apart the GyrA/B fusion construct and reversing the Y123F deactivation mutation due to its proximity to the binding site. However, the missing Greek-Key domains were not reconstructed. The set of 14 NBTIs (see below) was subsequently docked using the original atomic coordinates of the cocrystallized **148** molecules as a target.

Our previously published[15] amide-type NBTIs constituted 12 of the 14 docked NBTIs. Eight of the 12, compounds **88**, **89**, **101**, **103**−**105**, **113**, and **115** (Supporting Information Figure S3A), primarily cause SSBs ("SSB subset") while the other four, compounds **148**, **185**, **186**, and **189** (Supporting Information Figure S3B), lead to accumulation of both SSBs and DSBs ("DSB subset").[15] The remaining two compounds docked were the triazoles **342** (induces SSBs, Figures 3 and 5) and **276** (induces both SSBs and DSBs, Figures 3 and 4).

Analysis of the docked structures showed prototypical NBTI binding configurations for all 14 compounds (Figure 6A). Overlaying the ligand-bound crystal structure for compound **148** and the aligned crystal structure of compound **185** onto their docked counterparts showed only minor deviations in the binding pose (Figure 6B, C). Docking compound **88** resulted in an increased distance to the proximal D83 residues compared to a previous docking study but maintained no direct interaction with R122 (Figure 6D).[5,15,23] The remaining docked compounds showed varying degrees of interaction with the local binding site residues (Supporting Information Figure S4). There were no significant differences in any of these distances between the SSB and DSB subsets of the compounds (Figure 6E). Also of note is that the two triazole compounds were docked in a highly similar manner, with a maximum deviation over all measured distances of only 0.3 Å in opposition to their different DNA cleavage patterns (Figure 6F).

The nonsignificant differences in binding pose distances across the SSB and DSB subsets, coupled with the nearly identical binding of the differentially DNA-cleaving triazole NBTIs, suggested that static docking alone is insufficient to identify potential explanations for differences in observed DNA cleavage patterns. To address this, the docked systems were used in an ensemble of molecular dynamics (MD) simulations. Each docked NBTI was simulated in triplicate 200 ns production simulations and seeded from separately minimized and equilibrated structures to randomize starting positions and velocities. The first 50 ns of each simulation were considered equilibration time and not analyzed (Supporting Information Figure S5).

We first examined the radius of gyration (R_{gyr}) as a metric for how conformationally dynamic each NBTI was throughout the simulation. This metric, aggregated over time, showed no significant difference between the SSB and DSB subsets, indicating little deviation from their initial binding pose. However, by isolating the horizontal components of R_{gyr}, we observed a significant difference between the groups (Figure 7A). It should be noted, however, that the triazole NBTIs possessed the highest average perpendicular R_{gyr} across both groups, indicating that high lateral bowing is not wholly predictive of DNA cleavage patterns. This is consistent with the observed horizontal bowing in the crystals of amide compounds **148** and **185** relative to other published structures[5,7,20,23,29,30] (*vide supra* and see Supporting Information Figure S6) and suggests that NBTI bowing is a feature of the oxazinone and thiazinone gyrase-binding moieties, rather than the amide or triazole motifs.

We next investigated specific NBTI-residue interactions, dividing the symmetric binding site into "Near" and "Far" residues based on proximity to the asymmetrically bound inhibitors (Figure 7B). Distances were collected at each simulation time step as the minimum between the atoms of the amide or triazole moieties and the functional groups of $D83_{Near/Far}$ and $R122_{Near/Far}$. Comparing the distances of the SSB and DSB subsets, averaged over time, revealed a significant difference for only Near-side residue R122 (Figure 7C). The per-compound distance distributions of $R122_{Near}$ (Figure 7D), aggregated over the three replicates, revealed that

https://doi.org/10.1021/acsmedchemlett.5c00060
ACS Med. Chem. Lett. 2025, 16, 660−667

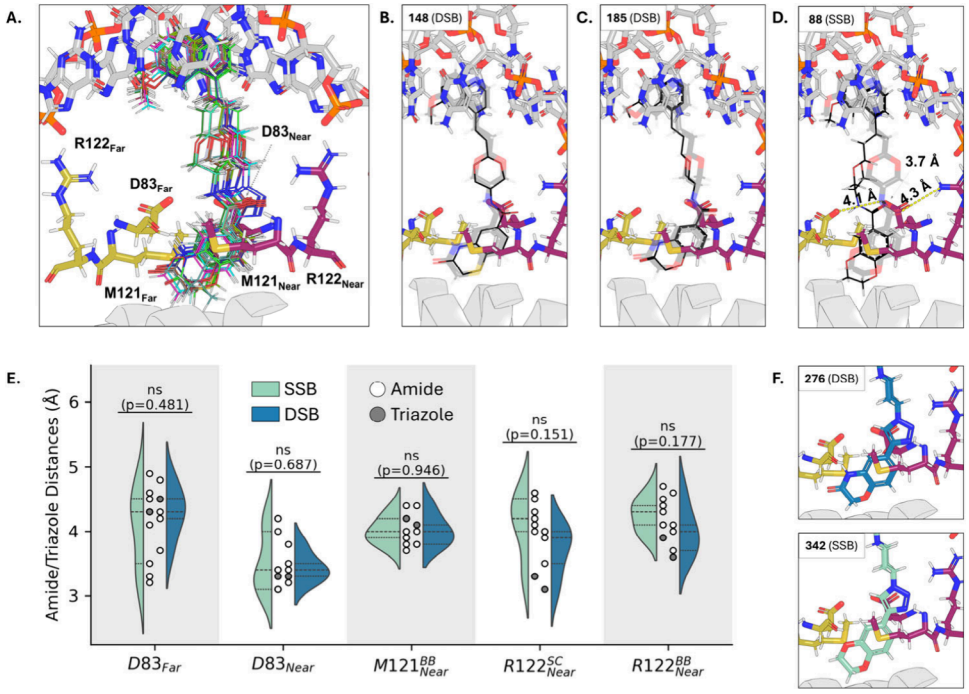

Figure 6. Computational docking results in the *S. aureus* DNA gyrase crystal resolved with **148**. (A) Compiled docked structures from all 14 compounds. Docked NBTIs are shown with a wire representation and binding site components shown as licorice. Symmetric binding site residues are labeled Near (magenta) and Far (yellow) based on their position relative to the bound NBTI. (B) Overlay of cocrystallized **148** (wire) with its docked pose (transparent). (C) Overlay of the aligned crystal of **185** (wire) with the docked pose (transparent). (D) Overlay of the previous docked pose of **88** in 2XCS (wire) and the newly docked pose (transparent). (E) Amide- and triazole-NBTI distance distributions to residue backbones (BB) and side chains (SC), grouped by SSB- (green) and DSB- (blue) subsets. Points show distances for individual NBTIs, color indicating an amide- or triazole-containing compound. (F) Docked poses of the two triazole NBTIs. **276** from the DSB-subset is in blue (top), and the SSB-subset **342** is in green (bottom). Statistical significance is given by an independent *t* test (* $p < 0.05$; ** $p < 0.01$; *** $p < 0.001$).

the distances of the DSB subset primarily fell into a bimodal distribution with peaks at around 3 and 5 Å. This contrasted with the irregular distributions of the SSB subset.

We speculate that the more consistent $R122_{Near}$ interactions for NBTIs in the DSB subset stem from their higher perpendicular R_{gyr}, as compounds with a more bowed pose could potentially interact with residues on the side of the binding pocket more frequently. Distance time-series of DSB-inducing **186** to $R122_{Near}$ showed a unique interaction pattern for each simulation replicate (Figure 7E, G). Distances remained stable at ∼ 3 and 5 Å for replicates 1 and 3, respectively, while replicate 2 alternated between these states. These interaction patterns underlie the bimodal distributions seen in Figure 7D. The stable 5 Å state corresponds to interactions between $R122_{Near}$ and the scissile phosphate group of the DNA backbone seen in our crystals of **148** and **185** as well as previously reported structures.[20] Supporting this, the time-series of $R122_{Near}$ and PO_4 distances for **186** followed a pattern nearly inverted to the amide distances (Figure 7F, G). It should be noted that the distances were not cleanly anticorrelated, as $R122_{Near}$ also interacted with other binding pocket elements (data not shown). However, both DSB-causing and SSB-causing triazole NBTIs appeared to bind so that $R122_{Near}$ formed a stable bridge between both Lewis basic nitrogens of the triazole and the backbone phosphate (Figure 7H). This, like perpendicular R_{gyr}, suggests that NBTI amide/triazole interactions with $R122_{Near}$ correlate with but do not drive different DNA cleavage patterns.

While the $D83_{Far}$ to NBTI-amide/triazole distances were not significantly different between the SSB and DSB subsets, the reason for the comparatively tight distribution of the DSB subset is unclear (Figure 7B). Given that a lower variance would most likely arise from a stabilizing interaction with an average distance of 5.1 Å, it was unlikely that contacts between the NBTI-amide/triazole motif and D83 were the source. Instead, we observed a stable interaction between $D83_{Far}$ and the oxazinone/thiazinone motifs of the DSB subset. This interaction has not been observed in experimental structures, but it was previously reported in docked poses of the oxazinone-containing BWC0977.[22] Distance distributions between $D83_{Far}$ and the oxazinone/thiazinone ring-nitrogen of the DSB group simulations showed stable interactions across replicates and were not observed in the SSB subset (Figure 7I, J). Unlike with the prior metrics, this specific interaction was possible for compound **276** but not for compound **342**. While we might speculate that the stabilization of $D83_{Far}$ alone causes the double stand breaks seen in this set of compounds, previous experimental studies comparing DNA cleavage between amide and amine analogues of oxazinone/thiazinone NBTIs only saw a substantial accumulation of double-strand DNA breaks in the amide compounds.[16] We thus hypothesize that specific interactions with both $R122_{Near}$ and $D83_{Far}$ are necessary to stabilize the doubly cleaved intermediate. Still, the mechanism through which these double strand breaks form remains elusive.

The canonical view of NBTIs suggests that they induce only single-strand DNA breaks, but exceptions have been reported.[15,16,31] X-ray crystal structures for two amide-type NBTIs previously shown to induce double-strand DNA breaks are presented. Each reveals an unusual binding mode, with a

https://doi.org/10.1021/acsmedchemlett.5c00060
ACS Med. Chem. Lett. 2025, 16, 660−667

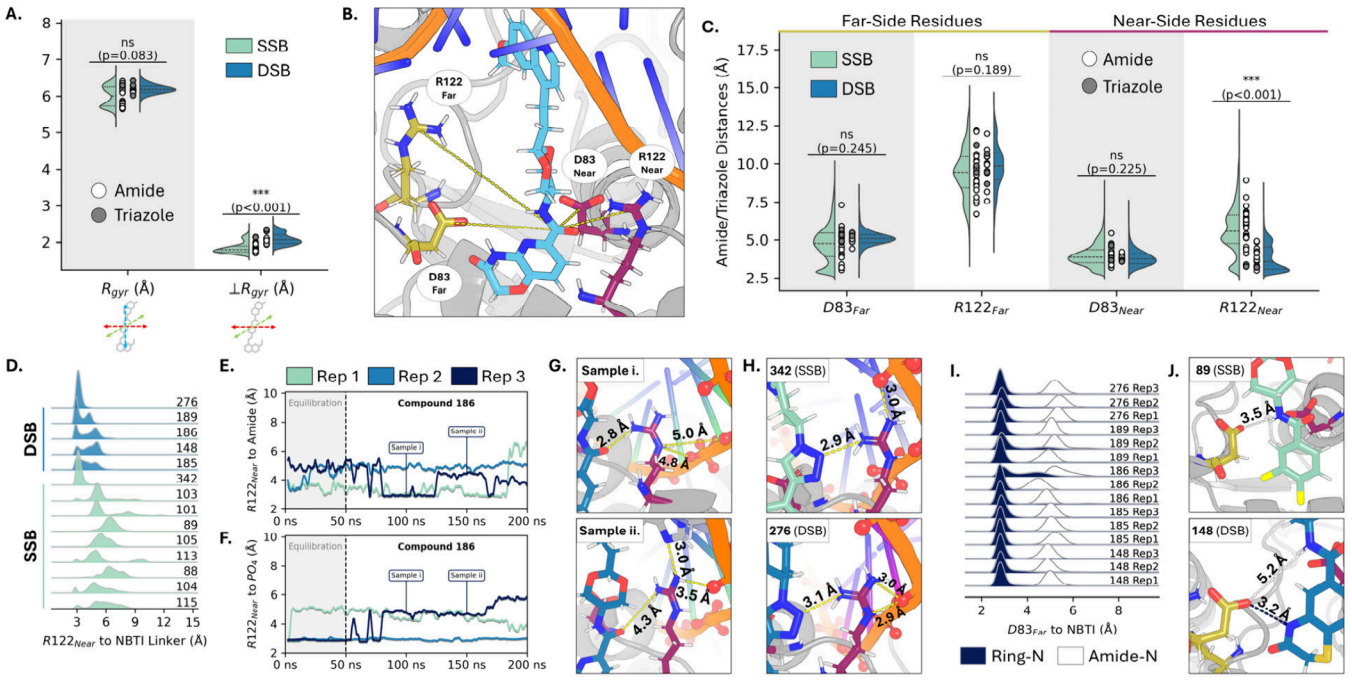

Figure 7. Molecular dynamics simulation analysis of NBTI functional group interactions with binding pocket residues. (A) Radius of gyration distributions split into SSB- and DSB-subsets. R_{gyr} denotes 3D radius of gyration, and $\perp R_{gyr}$ represents horizontal gyration, perpendicular to the longest axis of the NBTI. The points show trajectory-averaged values colored by NBTI linker motif. (B) Binding pocket map of the positions of the *Near*-side (magenta) and *Far*-side (yellow) residues relative to an NBTI (cyan). Dashed lines show distances measured throughout the simulations. Minimum distances between residue side chains and amide and triazole heavy-atoms were collected. (C) Aggregate distances measured throughout the simulation to the four interacting residues shown in part B. Average distances for each NBTI simulation replicate are shown as points colored by their motifs. (D) Per-compound distance distributions between $R122_{Near}$ and the NBTIs shown in part C. Each distribution contains distances from three replicate trajectories. Time-series distances of **186** over replicates between (E) the amide or triazole to the side chain of $R122_{Near}$ and (F) the guanidino group of $R122_{Near}$ to the scissile phosphate. Curves were smoothed by rolling average with a window size of 1% total trajectory length. Gray regions indicate the equilibration period excluded from analyses. (G) Representative distances sampled from the trajectory denoted in E & F at 100 ns (top) and 150 ns (bottom). **186** is shown in blue, $R122_{Near}$ in magenta, and the phosphate group oxygens in red. (H) Distances of the NBTI triazole and scissile phosphate to $R122_{Near}$, taken from the final frame of replicate 3 for **342** (top, green) and **276** (bottom, blue). (I) Per-replicate distance distributions between $D83_{Far}$ and different NBTI motifs. (J) Representative interaction distances of $D83_{Far}$ in yellow with SSB-inducing **89** in green (*Top*) and SSB- & DSB-inducing 148 in blue (*Bottom*). Statistical significance is given by the Mann−Whitney U-test for non-normal distributions (* $p < 0.05$; ** $p < 0.01$; *** $p < 0.001$).

bowed linker conformation and engagement of R122 in addition to D83, which commonly binds NBTIs. Two new triazole-type NBTIs reveal a divergence in DNA cleavage stabilization similar to the previously reported[15] amides, with an oxazinone-containing triazole inducing both single- and double-strand DNA breaks and a benzodioxane analogue affording only single-strand breaks. Molecular dynamics simulations suggest that oxazinone- and thiazinone-containing amide and triazole NBTIs have an additional hydrogen bonding interaction with D83. These results contribute to the understanding of the mechanism of action of this emerging class of antibacterial agents and illustrate the value of structural biology in drug discovery.

■ ASSOCIATED CONTENT

Supporting Information

The Supporting Information is available free of charge at https://pubs.acs.org/doi/10.1021/acsmedchemlett.5c00060.

Synthesis and characterization of triazoles **276** and **342**. Methods for X-ray crystallography, DNA cleavage experiments, docking, and molecular dynamics. Scheme S1, Table S1, and Figures S1−S6. ^{1}H and ^{13}C NMR spectra and UPLC chromatograms for **276** and **342** (PDF)

■ AUTHOR INFORMATION

Corresponding Author

Mark J. Mitton-Fry − *Division of Medicinal Chemistry and Pharmacognosy, College of Pharmacy, The Ohio State University, Columbus, Ohio 43210, United States of America;* orcid.org/0000-0002-6715-8836; Email: mitton-fry.1@osu.edu

Authors

Paul D. Toth − *Department of Chemistry and Biochemistry, College of Arts and Sciences, The Ohio State University, Columbus, Ohio 43210, United States of America;* orcid.org/0009-0003-3814-7657

Steven C. Ratigan − *Division of Medicinal Chemistry and Pharmacognosy, College of Pharmacy, The Ohio State University, Columbus, Ohio 43210, United States of America*

Joshua W. Powell − *Division of Medicinal Chemistry and Pharmacognosy, College of Pharmacy, The Ohio State University, Columbus, Ohio 43210, United States of America*

Sydney R. Cassel − *Division of Pharmaceutics and Pharmacology, College of Pharmacy, The Ohio State University, Columbus, Ohio 43210, United States of America*

https://doi.org/10.1021/acsmedchemlett.5c00060
ACS Med. Chem. Lett. 2025, 16, 660−667

Jack C. Yalowich − *Division of Pharmaceutics and Pharmacology, College of Pharmacy, The Ohio State University, Columbus, Ohio 43210, United States of America*

Craig A. McElroy − *Division of Medicinal Chemistry and Pharmacognosy, College of Pharmacy, The Ohio State University, Columbus, Ohio 43210, United States of America;* orcid.org/0000-0001-5950-0120

Steffen Lindert − *Department of Chemistry and Biochemistry, College of Arts and Sciences, The Ohio State University, Columbus, Ohio 43210, United States of America;* orcid.org/0000-0002-3976-3473

Charles E. Bell − *Department of Biological Chemistry and Pharmacology, College of Medicine, The Ohio State University, Columbus, Ohio 43210, United States of America*

Complete contact information is available at: https://pubs.acs.org/10.1021/acsmedchemlett.5c00060

Author Contributions

⊥Denotes cofirst authors.

Notes

The authors declare the following competing financial interest(s): M.J.M.-F. is a shareholder of Pfizer.

■ ACKNOWLEDGMENTS

The authors acknowledge funding from the National Institutes of Health grant R01 AI173072 and the Dr. Ralph and Marian Falk Medical Research Trust (Catalyst and Transformational Awards). We thank Dr. Yanran Lu for the initial syntheses of the previously reported amide derivatives.

■ ABBREVIATIONS USED

NBTI, novel bacterial topoisomerase inhibitor; SSB, single-strand break; DSB, double-strand break; hERG, human ether-related a-go-go gene; GKdel, Greek Key deletion

■ REFERENCES

(1) Murray, C. J.; et al. Global burden of bacterial antimicrobial resistance in 2019: A Systematic Analysis. *Lancet* **2022**, *399*, 629−655.

(2) Mitton-Fry, M. J. Novel Bacterial Type II Topoisomerase Inhibitors. *Med. Chem. Rev.* **2017**, *52*, 281−302.

(3) Kolarič, A.; Anderluh, M.; Minovski, N. Two Decades of Successful SAR-Grounded Stories of the Novel Bacterial Topoisomerase Inhibitors (NBTIs). *J. Med. Chem.* **2020**, *63*, 5664−5674.

(4) Collins, J. A.; Osheroff, N. Gyrase and Topoisomerase IV: Recycling Old Targets for New Antibacterials to Combat Fluoroquinolone Resistance. *ACS Infect. Dis.* **2024**, *10*, 1097−1115.

(5) Bax, B. D.; Chan, P. F.; Eggleston, D. S.; Fosberry, A.; Gentry, D. R.; Gorrec, F.; Giordano, I.; Hann, M. M.; Hennessy, A.; Hibbs, M.; Huang, J.; Jones, E.; Jones, J.; Brown, K. K.; Lewis, C. J.; May, E. W.; Saunders, M. R.; Singh, O.; Spitzfaden, C. E.; Shen, C.; Shillings, A.; Theobald, A. J.; Wohlkonig, A.; Pearson, N. D.; Gwynn, M. N. Type IIA Topoisomerase Inhibition by a New Class of Antibacterial Agents. *Nature* **2010**, *466*, 935−940.

(6) Bax, B. D.; Murshudov, G.; Maxwell, A.; Germe, T. DNA Topoisomerase Inhibitors: Trapping a DNA-Cleaving Machine in Motion. *J. Mol. Biol.* **2019**, *431*, 3427−3449.

(7) Gibson, E. G.; Bax, B.; Chan, P. F.; Osheroff, N. Mechanistic and Structural Basis for the Actions of the Antibacterial Gepotidacin against *Staphylococcus aureus* Gyrase. *ACS Infect. Dis.* **2019**, *5*, 570−581.

(8) Vanden Broeck, A.; Lotz, C.; Ortiz, J.; Lamour, V. Cryo-EM Structure of the Complete E. coli DNA Gyrase Nucleoprotein Complex. *Nat. Commun.* **2019**, *10*, 4935.

(9) Kolarič, A.; Germe, T.; Hrast, M.; Stevenson, C. E. M.; Lawson, D. M.; Burton, N. P.; Vörös, J.; Maxwell, A.; Minovski, N.; Anderluh, M. Potent DNA Gyrase Inhibitors Bind Asymmetrically to Their Target Using Symmetrical Bifurcated Halogen Bonds. *Nat. Commun.* **2021**, *12*, 150.

(10) Kokot, M.; Hrast Rambaher, M.; Feng, L.; Mitchenall, L. A; Lawson, D. M; Maxwell, A.; Parish, T.; Minovski, N.; Anderluh, M. Structural Aspects of *Mycobacterium tuberculosis* DNA Gyrase Targeted by Novel Bacterial Topoisomerase Inhibitors. *ACS Med. Chem. Lett.* **2024**, *15*, 2164−2170.

(11) Black, M. T.; Stachyra, T.; Platel, D.; Girard, A. M.; Claudon, M.; Bruneau, J. M.; Miossec, C. Mechanism of Action of the Antibiotic NXL101, a Novel Nonfluoroquinolone Inhibitor of Bacterial Type II Topoisomerases. *Antimicrob. Agents Chemother.* **2008**, *52*, 3339−3349.

(12) Mitton-Fry, M. J.; Brickner, S. J.; Hamel, J. C.; Brennan, L.; Casavant, J. M.; Chen, M.; Chen, T.; Ding, X.; Driscoll, J.; Hardink, J.; Hoang, T.; Hua, E.; Huband, M. D.; Maloney, M.; Marfat, A.; McCurdy, S. P.; McLeod, D.; Plotkin, M.; Reilly, U.; Robinson, S.; Schafer, J.; Shepard, R. M.; Smith, J. F.; Stone, G. G.; Subramanyam, C.; Yoon, K.; Yuan, W.; Zaniewski, R. P.; Zook, C. Novel Quinoline Derivatives as Inhibitors of Bacterial DNA Gyrase and Topoisomerase IV. *Bioorg. Med. Chem. Lett.* **2013**, *23*, 2955−2961.

(13) Surivet, J.-P.; Zumbrunn, C.; Rueedi, G.; Hubschwerlen, C.; Bur, D.; Bruyère, T.; Locher, H.; Ritz, D.; Keck, W.; Seiler, P.; Kohl, C.; Gauvin, J.-C.; Mirre, A.; Kaegi, V.; Dos Santos, M.; Gaertner, M.; Delers, J.; Enderlin-Paput, M.; Boehme, M. Design, Synthesis, and Characterization of Novel Tetrahydropyran-Based Bacterial Topoisomerase Inhibitors with Potent Anti-Gram-Positive Activity. *J. Med. Chem.* **2013**, *56*, 7396−7415.

(14) Lu, Y.; Vibhute, S.; Li, L.; Okumu, A.; Ratigan, S. C.; Nolan, S.; Papa, J. L.; Mann, C. A.; English, A.; Chen, A.; Seffernick, J. T.; Koci, B.; Duncan, L. R.; Roth, B.; Cummings, J. E.; Slayden, R. A.; Lindert, S.; McElroy, C. A.; Wozniak, D. J.; Yalowich, J. C.; Mitton-Fry, M. J. Optimization of TopoIV Potency, ADMET Properties, and hERG Inhibition of 5-Amino-1,3-dioxane-Linked Novel Bacterial Topoisomerase Inhibitors: Identification of a Lead with In Vivo Efficacy against MRSA. *J. Med. Chem.* **2021**, *64*, 15214−15249.

(15) Lu, Y.; Papa, J. L.; Nolan, S.; English, A.; Seffernick, J. T.; Shkolnikov, N.; Powell, J.; Lindert, S.; Wozniak, D. J.; Yalowich, J.; Mitton-Fry, M. J. Dioxane-Linked Amide Derivatives as Novel Bacterial Topoisomerase Inhibitors against Gram-positive *Staphylococcus aureus*. *ACS Med. Chem. Lett.* **2020**, *11*, 2446−2454.

(16) Mann, C. A.; Carvajal Moreno, J. J.; Lu, Y.; Dellos-Nolan, S.; Wozniak, D. J.; Yalowich, J. C.; Mitton-Fry, M. J. Novel Bacterial Topoisomerase Inhibitors: Unique Targeting Activities of Amide Enzyme-Binding Motifs for Tricyclic Analogs. *Antimicrob. Agents Chemother.* **2023**, *67*, e00482−23.

(17) Kokot, M.; Weiss, M.; Zdovc, I.; Senerovic, L.; Radakovic, N.; Anderluh, M.; Minovski, N.; Hrast, M. Amide Containing NBTI Antibacterials with Reduced hERG Inhibition, Retained Antimicrobial Activity against Gram-Positive Bacteria and *In Vivo* Efficacy. *Eur. J. Med. Chem.* **2023**, *250*, No. 115160.

(18) Mitton-Fry, M. J.; Cummings, J. E.; Lu, Y.; Armenia, J. F.; Byl, J. A. W.; Oviatt, A. A.; Bauman, A. A.; Robertson, G. T.; Osheroff, N.; Slayden, R. A. Anti-Mycobacterial Activity of Bacterial Topoisomerase Inhibitors with Dioxygenated Linkers. *ACS Infect. Dis.* **2025**, *11*, 474−482.

(19) Zumbrunn, C. A Short History of Topoisomerase Inhibitors at Actelion Pharmaceuticals. *Chimia* **2022**, *76*, 647−655.

(20) Cumming, J. G.; Kreis, L.; Kühne, H.; Wermuth, R.; Vercruysse, M.; Kramer, C.; Rudolph, M. G.; Xu, Z. Discovery of a Series of Indane-Containing NBTIs with Activity against Multidrug-Resistant Gram-Negative Pathogens. *ACS Med. Chem. Lett.* **2023**, *14*, 993−998.

(21) Cumming, J. G.; Kreis, L.; Kühne, H.; Wermuth, R.; Vercruysse, M.; Cantrill, C.; Bissantz, C.; Qiu, H.; Kramer, C.; Andreotti, D.; Fossati, G. Novel Indane-containing NBTIs with

Potent Anti-Gram-Negative Activity and Minimal hERG Inhibition. *ACS Med. Chem. Lett.* **2023**, *14*, 1791−1799.
(22) Hameed P, S.; Kotakonda, H.; Sharma, S.; Nandishaiah, R.; Katagihallimath, N.; Rao, R.; Sadler, C.; Slater, I.; Morton, M.; Chandrasekaran, A.; Griffen, E.; Pillai, D.; Reddy, S.; Bharatham, N.; Venkatesan, S.; Jonnalagadda, V.; Jayaraman, R.; Nanjundappa, M.; Sharma, M.; Raveendran, S.; Rajagopal, S.; Tumma, H.; Watters, A.; Becker, H.; Lindley, J.; Flamm, R.; Huband, M.; Sahm, D.; Hackel, M.; Mathur, T.; Kolamunnage-Dona, R.; Unsworth, J.; Mcentee, L.; Farrington, N.; Manickam, D.; Chandrashekara, N.; Jayachandiran, S.; Reddy, H.; Shanker, S.; Richard, V.; Thomas, T.; Nagaraj, S.; Datta, S.; Sambandamurthy, V.; Ramachandran, V.; Clay, R.; Tomayko, J.; Das, S.; V, B. BWC0977, a Broad-Spectrum Antibacterial Clinical Candidate to Treat Multidrug Resistant Infections. *Nature Commun.* **2024**, *15*, 8202.
(23) Magaro, G.; Prati, F.; Garofalo, B.; Corso, G.; Furlotti, G.; Apicella, C.; Mangano, G.; D'Atanasio, N.; Robinson, D.; Di Giorgio, F. P.; Ombrato, R. Virtual Screening Approach and Investigation of Structure-Activity Relationships to Discover Novel Bacterial Topoisomerase Inhibitors Targeting Gram-Positive and Gram-Negative Pathogens. *J. Med. Chem.* **2019**, *62*, 7445−7472.
(24) Kolarič, A.; Minovski, N. Novel Bacterial Topoisomerase Inhibitors: Challenges and Perspectives in Reducing hERG Toxicity. *Future Med. Chem.* **2018**, *10*, 2241−2244.
(25) Morgan, H.; Nicholls, R. A.; Warren, A. J.; Ward, S. E.; Evans, G.; Long, F.; Murshudov, G. N.; Duman, R.; Bax, B. D. How do Gepotidacin and Zoliflodacin Stabilize DNA Cleavage Complexes with Bacterial Type IIA Topoisomerases? 1. Experimental Definition of Metal Binding Sites. *Int. J. Mol. Sci.* **2024**, *25*, 11688.
(26) Nicholls, R. A.; Morgan, H.; Warren, A. J.; Ward, S. E.; Long, F.; Murshudov, G. N.; Sutormin, D.; Bax, B. D. How do Gepotidacin and Zoliflodacin Stabilize DNA-Cleavage Complexes with Bacterial Type IIA Topoisomerases? 2. A single Moving Metal Mechanism. *Int. J. Mol. Sci.* **2025**, *26*, 33.
(27) Germe, T.; Vörös, J.; Jeannot, F.; Taillier, T.; Stavenger, R. A.; Bacqué, E.; Maxwell, A.; Bax, B. D. A New Class of Antibacterials, the Imidazopyrazinones, Reveal Structural Transitions Involved in DNA Gyrase Poisoning and Mechanisms of Resistance. *Nucleic Acids Res.* **2018**, *46*, 4114−4128.
(28) Kumari, S.; Carmona, A. V.; Tiwari, A. K.; Trippier, P. C. Amide Bond Isosteres: Strategies, Synthesis, and Successes. *J. Med. Chem.* **2020**, *63*, 12290−12358.
(29) Miles, T. J.; Hennessy, A. J.; Bax, B.; Brooks, G.; Brown, B. S.; Brown, P.; Cailleau, N.; Chen, D.; Dabbs, S.; Davies, D. T.; Esken, J. M.; Giordano, I.; Hoover, J. L.; Jones, G. E.; Kusalakumari Sukmar, S. K.; Markwell, R. E.; Minthorn, E. A.; Rittenhouse, S.; Gwynn, M. N.; Pearson, N. D. Novel Tricyclics (e.g., GSK945237) as Potent Inhibitors of Bacterial Type IIA Topoisomerases. *Bioorg. Med. Chem. Lett.* **2016**, *26*, 2464−2469.
(30) Singh, S. B.; Kaelin, D. E.; Wu, J.; Miesel, L.; Tan, C. M.; Black, T.; Nargund, R.; Meinke, P. T.; Olsen, D. B.; Lagrutta, A.; Lu, J.; Patel, S.; Rickert, K. W.; Smith, R. F.; Soisson, S.; Sherer, E.; Joyce, L. A.; Wei, C.; Peng, X.; Wang, X.; Fukuda, H.; Kishii, R.; Takei, M.; Takano, H.; Shibasaki, M.; Yajima, M.; Nishimura, A.; Shibata, T.; Fukuda, Y. Tricyclic 1,5-Naphthyridinone Oxabicyclooctane-Linked Novel Bacterial Topoisomerase Inhibitors as Broad-Spectrum Antibacterial Agents-SAR of Left-Hand-Side Moiety (Part-2). *Bioorg. Med. Chem. Lett.* **2015**, *25*, 1831−1835.
(31) Dauda, S. E.; Collins, J. A.; Byl, J. A. W.; Lu, Y.; Yalowich, J. C.; Mitton-Fry, M. J.; Osheroff, N. Actions of a Novel Bacterial Topoisomerase Inhibitor against *Neisseria gonorrhoeae* Gyrase and Topoisomerase IV: Enhancement of Double-Stranded DNA Breaks. *Int. J. Mol. Sci.* **2023**, *24*, 12107.

https://doi.org/10.1021/acsmedchemlett.5c00060
ACS Med. Chem. Lett. 2025, 16, 660−667